Transport and noise properties of graphene-based transistors revealed through atomistic modelling

G. Iannaccone*, A. Betti, G. Fiori
Dipartimento Ingegneria dell'Informazione: Elettronica, Informatica e Telecomunicazioni,
Università di Pisa, Via Caruso 16, 56122, Pisa, Italy
Tel: +39 050 2217677, Fax: +39 050 2217522, *email: g.iannaccone@unipi.it

Abstract

We discuss an intriguing set of transport and noise properties of graphene-based transistors that can be investigated in a direct way with atomistic modeling - Non-Equilibrium Green's Functions with a Tight-Binding Hamiltonian - and are not directly accessible with models based on a higher level of physical abstraction. We present an investigation of the achievable electron mobility in channels based on graphene nanoribbons with realistic imperfections. Then, we will discuss how the small gap and small density of states of bilayer graphene can be used to design tunnel FETs with extremely steep subthreshold slope. Then, as far as noise is concerned, we will show the impact of electron-electron interaction and of interband transitions in enhancing the channel noise of FETs based on small-gap carbon nanotubes.

Introduction

The interest of the scientific community in graphene-based electronics is ignited by impressive and promising experiments [1-3]. Also because of the relative novelty of this research field, several aspects need to be understood to assess the realistic perspectives of carbon as an alternative to silicon technology.
In this context, numerical simulations are essential for understanding transport in carbon-based devices and evaluating technological challenges and opportunities, especially now that controlled and reproducible experiments are certainly not abundant.
In this work, we show the possibilities offered by atomistic simulations in understanding transport and noise properties of graphene-based transistors.

Methodology

First, we would like to mention the physical model at the core of our parallelized 3D device simulator NanoTCAD ViDES [4]. The three-dimensional Poisson equation reads

$$\nabla\left[\epsilon(\vec{r})\nabla\phi(\vec{r})\right] = -q\left[p(\vec{r}) - n(\vec{r}) + N_D^+(\vec{r}) - N_A^-(\vec{r}) + \rho_{fix}\right]$$

where ϕ is the electrostatic potential, q is the elementary charge, ε is the dielectric constant, N_D^+ and N_A^- are the concentration of the ionized donors and acceptors, respectively, ρ_{fix} is the fixed charge. Electrons and holes concentrations n and p, respectively, are computed with the NEGF formalism, using a tight-binding Hamiltonian with an atomistic (p_z orbitals) real space basis set with a hopping parameter t = 2.7 eV. The Green's function can then be expressed as

$$G(E) = [EI - H - \Sigma_S - \Sigma_D]^{-1}$$

where E is the energy, I the identity matrix, H the Hamiltonian, and Σ_S and Σ_D are the self-energies of the source and drain, respectively.
A point charge approximation is assumed, i.e. all the free charge around each carbon atoms is spread with a uniform concentration in the elementary cell including the atom. In particular, the electron and hole densities are computed from the Density of States (DOS), derived through the NEGF formalism. Assuming that the chemical potential of the reservoirs are aligned at the equilibrium with the flat Fermi level of the CNT, and given that there are no fully confined states, we have

$$\begin{aligned} n(\vec{r}) &= 2\int_{E_i}^{+\infty} dE\,[\mathrm{DOS_S}(\mathrm{E},\vec{\mathrm{r}})f(E-E_{F_S}) \\ &\quad +\mathrm{DOS_D}(\mathrm{E},\vec{\mathrm{r}})f(E-E_{F_D})]\,, \end{aligned}$$

and

$$\begin{aligned} p(\vec{r}) &= 2\int_{-\infty}^{E_i} dE\,\{\mathrm{DOS_S}(\mathrm{E},\vec{\mathrm{r}})\,[1-f(E-E_{F_S})] \\ &\quad +\mathrm{DOS_D}(\mathrm{E},\vec{\mathrm{r}})\,[1-f(E-E_{F_D})]\}\,, \end{aligned}$$

where f is the Fermi-Dirac occupation factor, DOS_S (DOS_D) is the density of states injected by the source (drain), and E_{FS} (E_{FD}) is the Fermi level of the source (drain). The current is expressed by means of the Landauer formula

$$I = \frac{2q}{h}\int_{-\infty}^{+\infty} dE\mathcal{T}(E)\,[f(E-E_{F_S}) - f(E-E_{F_D})]$$

where h is Planck's constant and T is the transmission coefficient. Particular attention must be put in the definition of each self-energy matrix: in our case we have considered a self-energy for semi-infinite leads as boundary condition for the Schrödinger equation.

Mobility in GNR-FETs

We have performed atomistic simulations of GNR-FETs over a wide range of GNR widths (W from 1 to 10 nm), including line-edge roughness (LER), defects, ionized impurities, acoustic and optical phonons. In particular, our approach is based on statistical simulations performed on large ensembles of actual distribution of non-idealities [5]. We compute mobility through computation of resistance on an ensemble of about 100 nanoribbon segments with different actual distribution of non-idealities as

$$\mu_n = \frac{L^2}{\langle R_{ch,i} - R_B\rangle\langle Q_i\rangle}\,,$$

where L is the segment length, Q_i and $R_{ch,i}$ are the total charge and the resistance of the i-th simulated GNR segment, respectively, R_B is the resistance of a ballistic segment in the same bias conditions and < > denotes the statistical average on the ensemble.
We model defects by computing the on-site energy and the hopping parameter of the Hamiltonian from DFT cal-

culations [6], and edge-disordered ribbons by randomly removing atoms on the two outermost dimer lines. For ionized impurities in the dielectric layer, we assume a point charge approximation. We obtain phonon-limited mobility from the Kubo-Greenwood formula as in [7].

The LER mobility (μ_{LER}) as a function of W for different edge-defect concentrations H is shown in Figure 1a in the above-threshold regime, for a 2D carrier density n_{2D} of 9×10^{12} cm^{-2}. The error bars represent the estimation of standard deviation of the error on the average of the statistical sample.

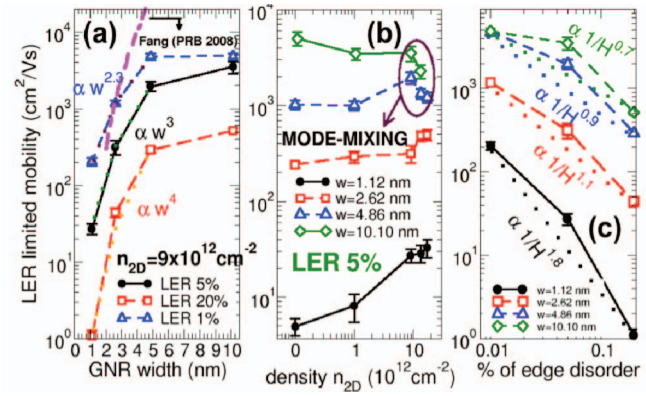

Fig. 1. a) LER-limited mobility as a function of W for an electron density $n_{2D} = 0.9 \times 10^{13}$ cm^{-2} and for different H, the fraction of vacancies at the edge. Data extracted from [7] are also reported. b) LER-limited mobility as a function of n_{2D} for H = 5%. c) LER-limited mobility as a function of edge disorder concentration H for $n_{2D} = 0.9 \times 10^{13}$ cm^{-2} and for different GNR width W.

As predicted by the analytical model in [7], μ_{LER} scales as W^4. Such behavior holds for large H (20%) and narrow GNRs (W < 5 nm), when scattering from edge defects is expected to be more severe. Deviations occur for wider GNRs and for smaller H. As shown in Figure 1b, in narrower GNRs the higher the electron density, the larger the effective mobility, because of stronger screening. As already observed in Silicon Nanowire FETs [8], μ_{LER} decreases for high n_{2D} and wider GNRs, due to mode-mixing.

Figure 1c shows μ_{LER} as a function of H, where $\mu_{LER} \propto 1/H$ for wide GNRs, as also observed in graphene in the presence of defects [9]. However, as soon as W decreases, quantum localization becomes relevant, and the Anderson insulator behavior is recovered, in agreement with analytical predictions.

We plot defect-limited mobility in Figure 2 as a function of W for different defect concentrations. Even in this case, localization affects mobility in narrower ribbons, especially for higher defect concentration (2.5%).

In Fig. 3, we compare the total mobility with experiments from Wang et al. [10]. In particular, we show mobility limited by different scattering mechanisms as well as the total mobility computed by means of Mathiessen's rule. As can be seen, when using phonon parameters as in [7], LER is the most limiting mechanism (H = 5%) for very narrower GNRs, whereas for wider GNRs defect scattering is predominant, if we consider a defect percentage of 0.5%. In addition, impurity scattering has only a minor effect on mobility in GNRs.

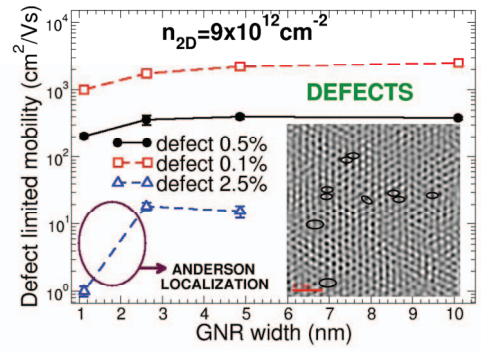

Fig. 2. Defect-limited mobility as a function of W for $n_{2D} = 9 \times 10^{12}$ cm^{-2} and for different defect percentage. In the inset, a TEM image of a graphene flake, where defects are highlighted is shown [5].

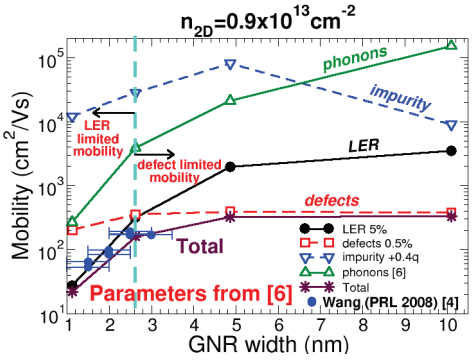

Fig. 3. Mobility limited by phonons, LER, defect and impurity scattering in the inversion regime for a LER concentration of 5%, and a defect concentration of 0.5%. The parameters for the scattering rates have been taken from [7]. The experimental mobility from [10] is also reported. $n_{2D} = 0.9 \times 10^{13}$ cm^{-2}, and the impurity concentration is 10^{12} cm^{-2}.

Bilayer-Graphene Tunnel FET

Graphene presents a serious problem and a possible showstopper for electronic applications: it has a zero bandgap. Very recent theoretical and experimental papers [11-12] have shown the possibility of inducing an energy gap (E_{gap}) in bilayer graphene by means of an applied electric field perpendicular to the graphene plane. This property could open the possibility of fabricating carbon-based electron devices, for which a semiconducting gap is required, with state-of-the-art lithography.

Atomistic simulations allow us to investigate the technology perspectives of a bilayer-graphene Tunnel FET (BG-TFET), whose device structure is shown in Fig. 4 [13]. The device has two independent control gates, biased with voltages V_{top} and V_{bottom}. The channel length L is 40 nm, and the p+ and n+ reservoirs are 40 nm long and doped with molar fraction f. Bilayer graphene is embedded in a 3-nm-thick SiO_2 insulator with relative dielectric constant $\varepsilon_r = 3.9$.

In Fig. 5 we show the transfer characteristics as a function of V_{bottom} of a device with molar fraction f = 2.5×10^{-3}, for fixed differential gate voltages $V_{diff}=V_{top}-V_{bottom}$ = 6, 6.5, 7, and 8 V. Differently from double-gate BG-FETs [14], the BG-TFET can be perfectly switched off, with a steep subthreshold behavior (always smaller than 20 mV/dec) and a large I_{on}/I_{off} ratio also for a very low V_{DD} (e.g., I_{on}/I_{off} = 4888 for V_{diff} = 8 V).

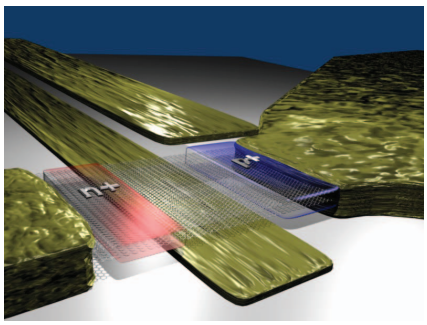

Fig. 4. Illustration of the simulated BG-TFET. Two gates are considered, one at the top (V_{top}) and one at the bottom (V_{bottom})

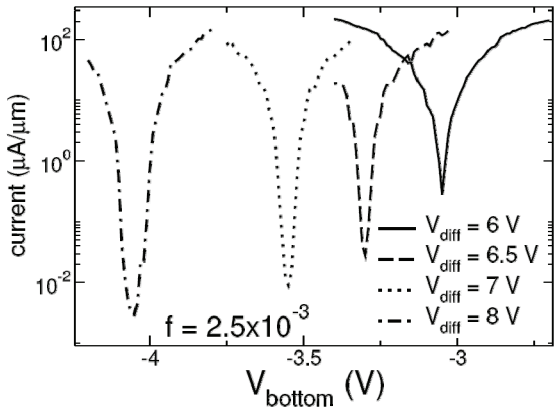

Fig. 5. Transfer characteristics of the double-gate BG-TFET for different $V_{diff}=V_{top}-V_{bottom}$. $f = 2.5\times10^{-3}$ and $V_{DS} = 0.1$V.

Due to the large vertical electric field applied to the structure, we need to examine the gate leakage current. We can estimate its value using a well-tested analytical model for Si−SiO_2 gate stacks based on WKB approximation of the triangular barrier. We find that 3-nm gate oxide is sufficient to obtain a gate current of the order of 10^{-6} μA/μm for $V_{diff} = 7$ V, and 10^{-4} μA/μm for $V_{diff} = 8$ V, i.e., negligible with respect to the smallest drain currents considered in our simulations.

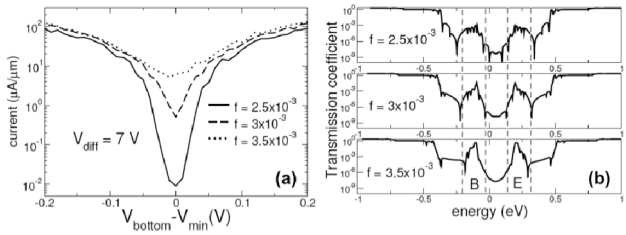

Fig. 6. a) Transfer characteristics of BG-TFETs for $V_{diff} = 7$ V, $V_{DS} = 0.1$ V, and different molar fractions f. $V_{min} = -3.55$ V. b) Transmission coefficient as a function of energy, for different molar fractions.

In Fig. 6a, we show the transfer characteristics as a function of V_{bottom}, for $V_{diff} = 7$ V, and for different dopant molar fractions f in the drain and source leads. As f is increased, the I_{on}/I_{off} ratio degrades, since I_{off} increases, while I_{on} remains almost constant. In Fig. 6b we show the transmission coefficient as a function of energy for different molar fraction. As the molar fraction increases, the tunneling components at the source and drain region increase, justifying the increase of the off-current.

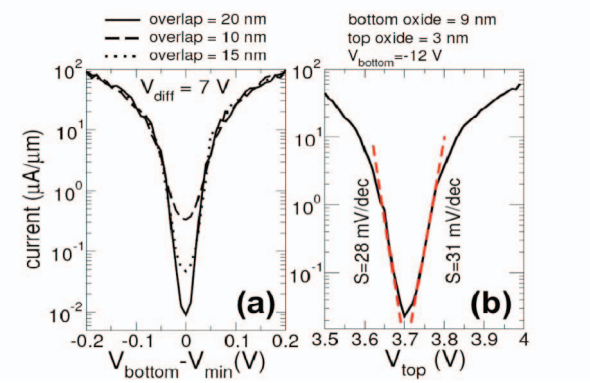

Fig. 7. a) Transfer characteristics of BG-TFET for $V_{diff} = 7$ V, $V_{DS} = 0.1$ V, and different gate overlap. $V_{min} = -3.55$ V. b) Transfer characteristic for a device with asymmetric oxide thicknesses: The top oxide thickness is 3 nm, and the bottom oxide thickness is 9 nm. V_{bottom} is fixed to −12 V and $V_{DS} = 0.1$ V.

In Fig. 7b, we show the transfer characteristics as a function of gate overlap. As shown, the smaller the overlap, the higher the I_{off} current.

In order to investigate the performance of single-gate devices, we have also performed simulations of a device with asymmetric gate oxide thicknesses [Fig. 7b]: the top oxide is 3 nm, and the bottom oxide is 9 nm. In this case, the bottom gate voltage is kept at a constant bias of −12 V, whereas the top gate is used as the control gate. This solution, with a common back gate at constant voltage for all FETs, is obviously more suitable for circuit integration. As can be noted, an I_{on}/I_{off} ratio of few hundred can be still obtained. The subthreshold swing (and then the I_{on}/I_{off} ratio) can be improved with a thicker bottom oxide of the order of 100 nm, which would reduce the capacitive coupling between channel and bottom gate.

Shot noise in ballistic carbon-based FETs

Atomistic modeling can also be used to investigate channel noise in ballistic FETs with carbon channels. We have recently developed a new methodology to investigate shot noise in nanoscale FETs, based on Monte Carlo simulations of randomly injected electrons from the reservoirs [15-16]. The main advantage of our approach is the capability to include electron-electron interaction, both through Pauli exclusion, and through the Coulomb force.

Let's call O_{Sm} (O_{Dm}) the random occupation at source S (drain D) contact for the mode m: it can be either 0 or 1, with a mean value equal to the Fermi statistic of the source f_S (f_D). Equivalently, we can define the source-to-drain (drain-to-source) transmission occurrence Ω_{mn} (Ω'_{mn}) from mode n to m, whose mean value is T_{mn} (T_{mn}'), the transmission coefficient from mode n to m.

From a computational point of view, O_{Sm} (Ω_{mn}) is obtained by extracting a random number r with uniform distribution between 0 and 1: if $r<f_S(E)$ ($r<T_{mn}(E)$) then $O_{Sm} = 1$ ($\Omega_{mn} = 1$), otherwise $O_{Sm} = 0$ ($\Omega_{mn} = 0$) .

The randomized current can then be expressed as:

$$I = \frac{e\,dE}{2\pi\hbar} \sum_{m\in S} \sum_{n\in D} \left[O_{Sm}\,\Omega_{nm} - O_{Dn}\,\Omega'_{mn} \right]$$

where dE is the energy step. By computing the statistical properties of the randomized current on a large ensemble of occurrencies, and by applying the formula discussed and derived in Refs. 15 and 16, we are able to compute the current noise power spectral density S and the so-called Fano factor $F = S/(2qI)$, i.e. the ratio of S to the power spectral density of a purely Poissonian process.

The approach is general and can be applied to any ballistic conductor. Here, we want to discuss results of its application to a double-gate Carbon NanoTube (CNT) FET. The channel consists of a zig-zag (25,0) CNT with a band gap E_{gap}= 0.39 eV and a diameter of 2 nm. The oxide thickness is 1 nm, the channel is undoped and has a length L of 10 nm. Source and drain extensions have a length of 10 nm and are doped with a molar fraction f=5x10^{-3}. For comparison purposes, we also consider a (13,0) CNT-FET, with E_{gap} = 0.75 eV, same geometry and doping profile.

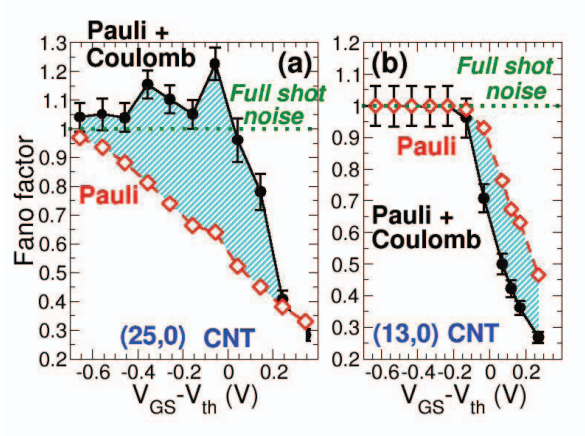

Fig. 8. a) Fano factor as a function of the gate overdrive for a (25,0) and b) (13,0) CNT-FETs for V_{DS}=0.5 V. The threshold voltage V_{th} is 0.43 V for the (13,0) CNT-FET, and 0.36 V for the (25,0) CNT-FET.

The Fano factor for a (25,0) and a (13,0) zig-zag CNT is plotted as a function of gate overdrive in Figs 8a and 8b. Noise enhancement occurs only in the case of the (25,0) CNT. If one neglects Coulomb interaction among carriers, the Fano factor is smaller than one. The whole shaded area in Fig. 8a predicts a shot noise enhancement due to Coulomb interaction [17]. This surprising behavior has yet to be observed experimentally.

Shot noise enhancement in the (25,0) CNT-FET can be explained with the help of Fig. 9. E_C and E_V are the conduction and valence band edge profiles in the channel, respectively, whereas E_{CS} (E_{CD}) is the conduction band edge at the source (drain), and E_{BS} is the energy level of the quasi-bound state in the valence band. When the drain Fermi level E_{FD} roughly aligns with E_{BS}, holes in the conduction band in correspondence of the drain can tunnel into the bound state shifting downwards E_C in the channel. As a result, thermionic electrons injected from the source can more easily overcome the barrier. Instead, when a hole leaves the bound state, the barrier increases by the same amount, reducing thermionic injection. The noise enhancement is fully due to current modulation due to trapping/detrapping of holes in the bound state. Since (13,0) CNTs have a much wider gap E_{gap} =0.75 eV, E_V in the channel is always below E_{CD} in the drain, and hole injection is completely inhibited, as well as noise enhancement.

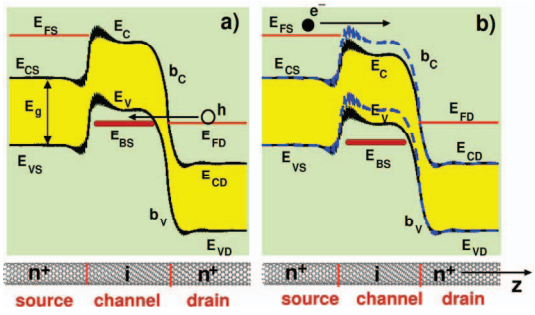

FIG. 9. If an excess hole tunnels from the drain into a bound state in the intrinsic channel (a), the conduction band E_C and valence band E_V edge profiles are shifted downwards and more thermionic electrons can be injected in the channel, enhancing current fluctuations (b).

Conclusion

The availability of affordable computational resources and of reliable libraries for parallel computation makes it possible to perform statistical atomistic simulations of complete devices. Carbon is particularly suitable for atomistic modeling, given the relatively simple and accurate tight-binding Hamiltonian. We have shown that atomistic simulations represent a powerful tool for the investigation of transport properties of carbon-based channels, for the exploration of technology options for the realization of carbon-based transistors, and for a deep physical understanding of the noise properties of nanoscale transistorrs.

Acknowledgments

Authors gratefully acknowledge EC 7FP grants GRAND (Contract 215752) and NANOSIL (Contract 216171), and the MIUR-PRIN project “Modeling and simulation of graphene nanoribbon FETs for high-performance and low-power logic applications” (Contract 2008S2CLJ9).

[1] J.-H. Chen et al, Nature Nanotech., Vol. 3, p. 206, 2008.
[2] X. Li et al, Science, Vol. 319, p. 1229, 2008.
[3] Z. Chen et al., IEDM Tech. Digest, p. 509, 2008.
[4] Code and Documentation can be found at the URL: http://www.nanohub.org.tools/vides.
[5] A. Betti et al. IEDM Tech. Digest, p. 897, 2009.
[6] I. Deretzis et al., J. Phys.: Condens. Matter, Vol. 22, 095504, 2009.
[7] T. Fang et al., Phys. Rev. B, Vol. 78, p. 205403, 2008.
[8] S. Poli et al., IEEE Trans. Electron Dev., Vol. 55, p. 2968, 2008.
[9] J.H. Chen et al., Phys. Rev. Lett., Vol. 102, p. 236805,2009.
[10] X. Wang et al., Phys. Rev. Lett., Vol. 100, p. 206803, 2008.
[11] E. McCann et al., Phys. Rev. Lett., Vol. 96, 086805, 2006.
[12] J. Nilsson, et al., Phys. Rev. Lett., Vol. 97, p. 266801, 2006.
[13] G. Fiori et al,. IEEE EDL, Vol. 30, p. 1096, 2009.
[14] G. Fiori et al., IEEE EDL, Vol. 30, p. 261, 2009.
[15] A. Betti et al., IEEE TED, Vol. 56, p. 2137, 2009.
[16] A. Betti et al., Phys. Rev. B., Vol. 81, 035329, 2010.
[17] A. Betti et al., Appl. Phys. Lett., Vol. 95, 252108, 2009.